Optics and Lasers in Engineering 115 (2019) 100–106

Contents lists available at ScienceDirect

Optics and Lasers in Engineering

journal homepage: www.elsevier.com/locate/optlaseng

Effects of different annealing processes on optoelectronic and bending fatigue properties of AgZr and ITO/AgZr thin film metallic glass

C. M. Chang [a], H. K. Lin [b,*], U. G. Huang [b], H. A. Hong [b], J. C. Huang [a,c]

[a] Department of Materials and Optoelectronic Science, National Sun Yat-sen University, Kaohsiung, Taiwan, ROC
[b] Graduate Institute of Materials Engineering, National Pingtung University of Science and Technology, Pingtung, Taiwan, ROC
[c] Department of Materials Science and Engineering, Institute for Advanced Study, City University of Hong Kong, Kowloon, Hong Kong

ARTICLE INFO

Keywords:
Furnace annealing
Laser annealing
Thin film metallic glass
Bi-layered electrode

ABSTRACT

Transparent conducting oxide (TCO) films are widely used throughout the optoelectronics industry. The present study explores the optoelectronic responses of AgZr (AZ) and ITO/AgZr (IAZ) thin film metallic glasses (TFMGs) with different Ag and Zr compositions and processed by two different annealing methods, namely furnace annealing (FA) and laser annealing (LA). Among the various as-deposited AZ and IAZ films, the ITO/$Ag_{66}Zr_{34}$ (IA6Z) film has the highest optical transmittance (55.7%) and the lowest sheet resistance (145.8 Ω/□) For the FA samples, an annealing temperature of 300 °C results in the optimal optoelectronic properties, namely a transmittance of 68.4% and a sheet resistance of 47.2 Ω/□. For the LA samples, the optimal processing conditions (a pulse energy of 2.5 μJ and a repetition rate of 150 kHz) yield optical transmittance and sheet resistance values of 64.0% and 17.8 Ω/□ respectively. The optimal LA processing conditions increase the Haacke figure of merit of the IA6Z sample from 2.0×10^{-5} in the as-deposited condition to 6.5×10^{-4} Ω^{-1} under the annealed condition; corresponding to a 32.5-fold improvement. Finally, the relative change in resistivity ($\Delta R/R_0$, where R_0 is the initial resistivity, R_i is the measured resistivity after a certain number of cycles, and ΔR is $R_i - R_0$) of the as-deposited IA6Z sample following fatigue testing (10,000 cycles) with a bend radius of 7 mm ($\Delta R/R_0$=0.49) is significantly lower than that of a pure ITO film of roughly equivalent thickness ($\Delta R/R_0$=0.93).

1. Introduction

Transparent conducting oxide (TCO) films have outstanding optical transmittance and electric conductivity properties. As a result, they are extensively and ubiquitously applied to optoelectronics and semiconductor industries for various purposes, such as organic LEDs (OLEDs), flat panel displays (FPDs), low-emissivity (low-E) coatings, solar cells, and touch panels [1–7]. Among various available TCOs, indium tin oxide (ITO) is one of the most commonly used due to its high optical transmittance in the visible range and low electrical resistivity [8,9]. However, to minimize the sheet resistance, the ITO thickness should exceed 100 nm [10,11]. As a result, the device cost is remarkably increases. Moreover, ITO films are inherently brittle, and are hence prone to micro-cracking and an increased resistivity under the tensile and/or fatigue loads encountered under typical service conditions. Accordingly, the problem of minimizing the usage of indium in multilayer electrodes has attracted significant attention in the literature [12–14].

Various studies have shown that ITO-metal-ITO sandwich structures incorporating highly-conductive pure metallic films (e.g. Ag or Cu) not only reduce the ITO cost, but also result in superior electrical conductivity and optical transmittance properties in the visible light range [15–17]. ITO/thin film metallic glass (TFMG) bi-layer systems are also an effective means of reducing the ITO cost and maintaining a good optoelectronic performance given an appropriate design of the TFMG composition and thickness [18,19]. TFMGs have a high nucleation rate and a thickness much lower than that of the metal layers used in traditional ITO sandwich structures. Consequently, they have attracted great interest in the optoelectronics and semiconductor industries in recent years [20].

In addition to TFMGs, TFMG composites (TFMGCs) have also been proposed, and their pure metallic glass layer is replaced by a composite layer consisting of nanocrystalline phases [21,22]. TFMGCs have significantly different properties from those of conventional metals and alloys, such as Ni-Cr film [23]. Huang et al [24,25] showed that the amorphous structures have an inherently higher resistivity due to their random atomic packing and the existence of free volume and vacancies. In contrast, TFMGCs, with partially nanocrystal and glassy region, possess better electric conductivity and good mechanical property in Al-based and Ag-based TFMGs/TFMGCs system.

Many studies have shown that the optical and electrical properties of as-deposited metallic thin films can be improved by thermal treatment,

* Corresponding author.
E-mail address: hklin@mail.npust.edu.tw (H. K. Lin).

https://doi.org/10.1016/j.optlaseng.2018.11.009
Received 19 September 2018; Received in revised form 9 November 2018; Accepted 15 November 2018

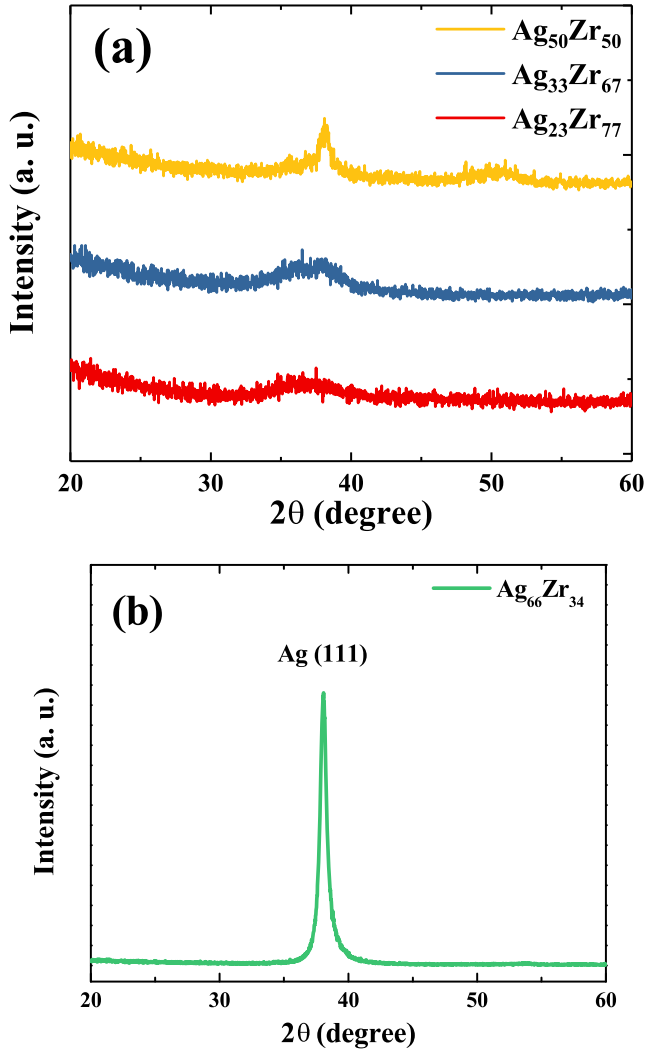

Fig. 1. X-ray diffraction scans of Ag-Zr monolithic films on glass substrate.

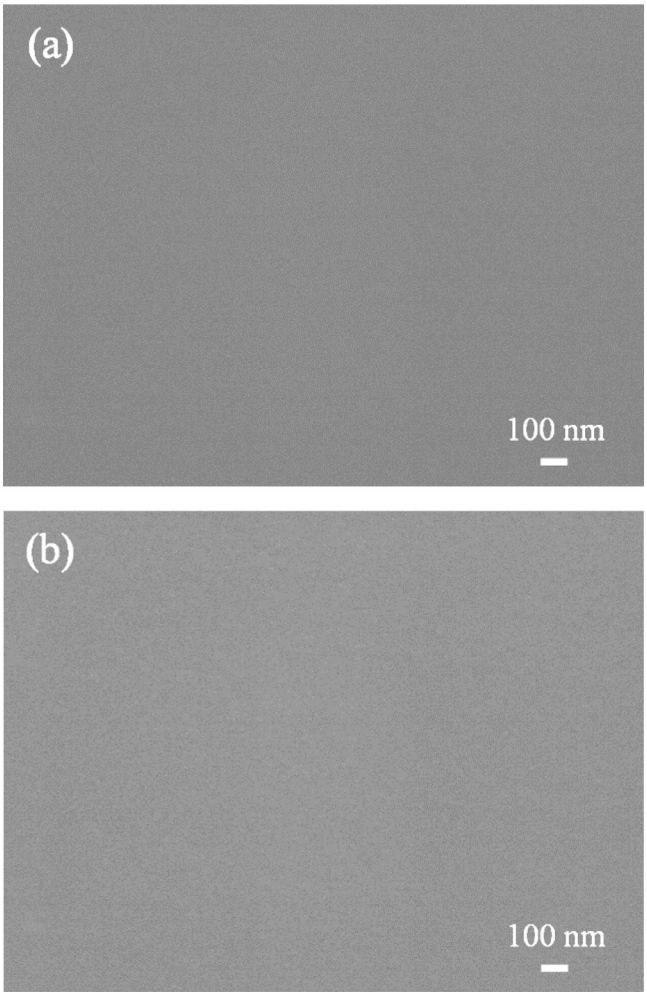

Fig. 2. Surface morphologies of as-deposited films: (a) $Ag_{66}Zr_{34}$ (A6Z) and (b) $Ag_{50}Zr_{50}$ (A5Z).

such as furnace annealing (FA) or laser annealing (LA) [26–31]. Moreover, the physical properties of TCO materials can be upgraded during the heat treatment [32,33], treating TCO films under high temperature (generally 400–700 °C) results in the elimination or even to recrystallization. However, traditional FA process involves treating whole workpieces in heat furnace. It is unsuitable for manufacturing products which consisted of the low melting materials such as glass or plastic substrate. In contrast, LA provides an efficient way to achieve local annealing TCO films to resolve the problems. With LA technology, photon energy is focused on the surface layer of the TCO films rather than the whole pieces. The temperature can rapid rise within a short time while the annealing effects can be achieved without damage to substrate by precisely control LA parameters [34–37].

Accordingly, the present study deposits AgZr (AZ) monolithic films and ITO/AZ (IAZ) bi-layer films with Ag contents ranging from 23 at% to 66 at% on glass substrates using a magnetron sputtering system. The optical and electronic properties of the AZ and IAZ films are investigated under the as-deposited condition and treated FA treatment at temperatures ranging from 100 °C–400 °C and LA processing with repetition rates ranging from 100–400 kHz and irradiation powers of 42–545 mW. Finally, the bending fatigue properties of the IAZ samples are examined by measuring the change in electrical resistivity during cyclic bending tests with a bend radius of 7 mm.

2. Experimental details

2.1. Sample preparation

AZ and IAZ films were deposited on glass substrates using a magnetron sputtering system (Kao Duen Co.) with Ag, Zr and ITO targets. The glass substrates were purchased from Nippon Electric Glass Co. (OA-10 G type) and had an optical transmittance of 92% for a normal incident wavelength of 550 nm. The Ag and Zr targets had purities of 99.99%, while the ITO target comprised 90 wt% In_2O_3 and 10 wt% SnO. All of the targets had a diameter of 50.8 mm and were sputtered at a working pressure of 5.0×10^{-3} torr. Prior to the deposition process, the chamber was evacuated to 2.0×10^{-6} torr and then backfilled with high purity Ar gas. To evaluate the effects of the film composition on the optical and electrical properties of the AZ and IAZ films, the discharge power of the Ag target was varied to obtain four different AZ films, namely $Ag_{66}Zr_{34}$ (denoted hereafter as A6Z), $Ag_{50}Zr_{50}$ (denoted as A5Z), $Ag_{33}Zr_{67}$ (denoted as A3Z) and $Ag_{23}Zr_{77}$ (denoted as A2Z), and to evaluate the effects of the film composition on the optical and electrical properties of the AZ and IAZ films. The compositions are expressed all in atomic percentage (at%) terms. For each AZ film, the sputtering time was carefully controlled to achieve a final film thickness of 10 nm. IAZ bi-layer films were then prepared by sputtering an ITO layer with a thickness of 30 nm on top of each AZ film.

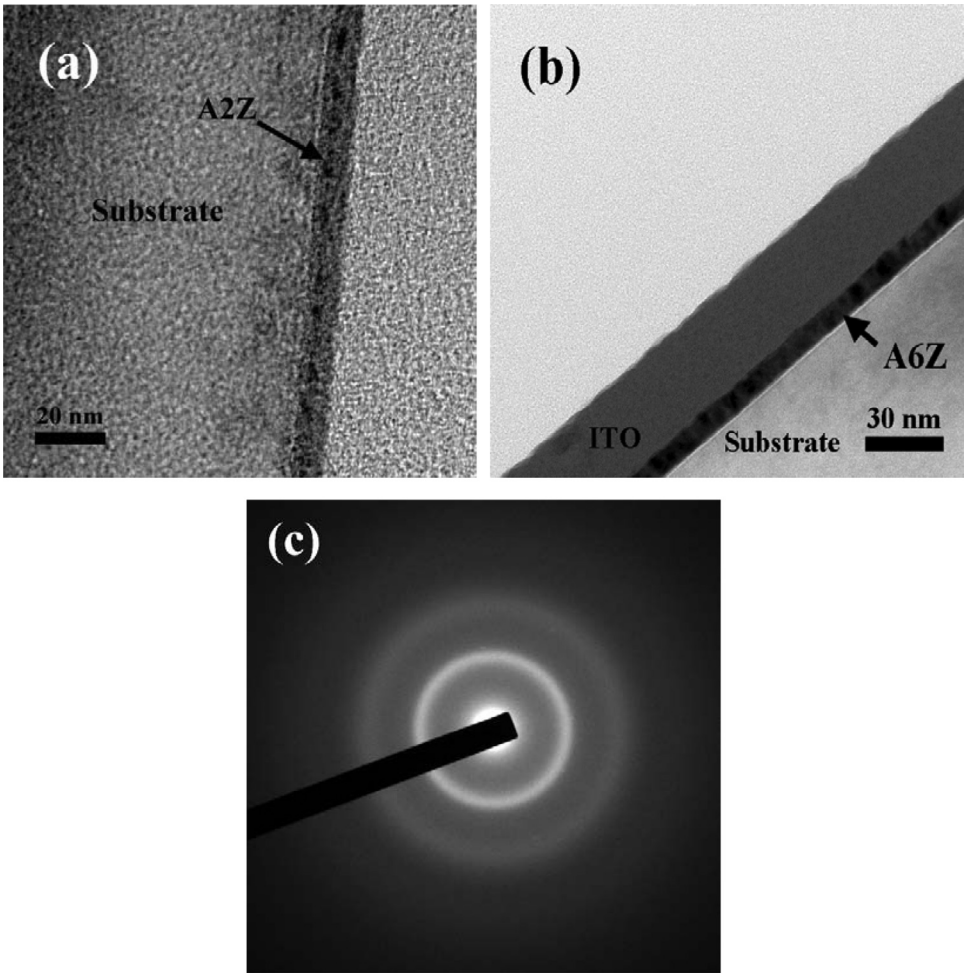

Fig. 3. TEM characterization results for as-deposited: (a) A2Z film, and (b) IA6Z film. (c) SAED of pure ITO layer.

Table 1
Sheet resistance, optical transmittance and figure of merit of as-deposited AZ and IAZ films with various compositions.

	Rs (Ω/□)	T (%)	ϕ_{TC} (Ω^{-1})
A2Z	1050.0	44.5	2.9×10^{-7}
A3Z	972.3	40.0	1.1×10^{-7}
A5Z	729.0	47.1	7.4×10^{-7}
A6Z	195.1	47.5	3.0×10^{-6}
IA2Z	927.4	51.0	1.3×10^{-6}
IA3Z	904.5	46.3	5.0×10^{-7}
IA5Z	609.3	52.5	2.6×10^{-6}
IA6Z	145.8	55.7	2.0×10^{-5}

2.2. Heat treatment

The as-deposited AZ and IAZ films were processed using two different annealing methods, namely furnace annealing (FA) and laser annealing (LA). To determine the optimal annealing parameters, the FA process was performed at various temperatures in the range of 100–400 °C with a heating rate of 5 °C/min and holding time of 1 h in every case to determine the optimal annealing parameters. Similarly, the LA process was conducted using a fiber laser (SPI-12, UK; 1064 nm wavelength) with repetition rates of 100~400 kHz and irradiation powers ranging from 42~545 mW. For all of the LA trials, the laser scanning speed was set as 5 mm/s, the laser spot size as 40 μm, and the pulse duration as 30 ns. The pulse energy (E) was evaluated as [38]

$$E = P_{AVG}/rep, \quad (1)$$

where P_{AVG} and rep denote the average power of the pulse laser and the laser repetition rate, respectively. For the irradiation powers and repetition rates considered in the present study, the pulse energy varied from 1.0 to 2.5 μJ.

2.3. Basic characterization

The sheet resistance (R_s) of the various AZ and IAZ films was measured using a four-point probe (SR-H1000C). In addition, the optical transmittance (T) was measured over the range of 200~1100 nm using a UV–vis-IR spectrophotometer (Lambda 35, PerkinElmer). The basic structures of the films were characterized by X-ray diffractometer (XRD, Bruker D8) by using monochromatic Cu-K_α radiation (λ€= 0.154 nm), with operational settings of 40 kV and 40 mA, respectively, and a 0.01 mm graphite monochromator. The morphologies and compositions of the various films were examined by scanning electron microscopy (SEM, JEOL JSM 7600F) and energy dispersive X-ray spectrometry (EDS), respectively. Cross-section TEM foils for microstructure observations were prepared using a dual-focus ion beam system (FIB, SEIKO SMI 3050) with an operating voltage of 30 kV and a 1 pA ion beam current. Phase identification was performed via analytical transmission electron microscopy (TEM, JEOL 3010) with an operating voltage of 200 kV.

The performance of the transparent conductive films was evaluated by means of the following figure of merit (FOM) (ϕ_{TC}) [39]:

$$\phi_{TC} = T^{10} / R_s, \quad (2)$$

where T is the transmittance (expressed in percentage terms) and R_s is the sheet resistance (measured in units of Ω/□). A higher FOM value

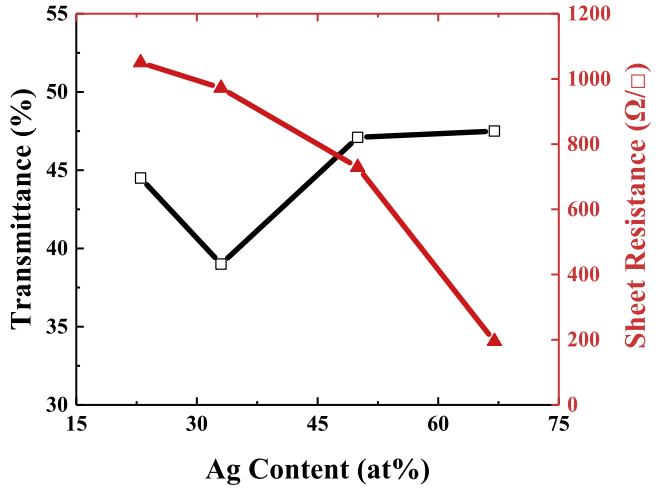

Fig. 4. Sheet resistance and optical transmittance of as-deposited AZ films.

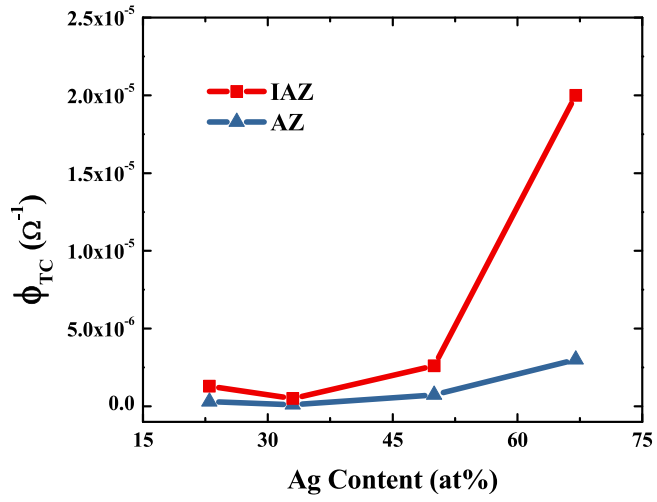

Fig. 5. Figure of merit values of as-deposited AZ and IAZ films.

indicates a better combination of transmittance (higher is better) and resistance (lower is better).

Finally, the fatigue properties of the IAZ samples were examined by measuring the change in electrical resistivity during cyclic bending tests. The tests were performed at a speed of 1 cycle/s with a bending curvature of R = 7 mm. The test specimens were deposited on PET substrates with a thickness of 50 μm. For each sample, the bending strain, ε, was calculated as

$$\varepsilon = h_s / 2R \times 100\%, \quad (3)$$

where h_s is the combined substrate and film thickness (PET substrate 50 μm). Therefore, the bending strain per cycle was therefore equal to 0.36%.

3. Results and discussion

3.1. Basic characterization of as-deposited films

Fig. 1(a) presents the XRD patterns of the as-deposited A2Z, A3Z and A5Z films. For all of the films, the XRD patterns are dominated by broad diffused humps, which indicate that the films have an amorphous structure. By contrast, the A6Z sample exhibits a strong peak at 38° (see Fig. 1(b)). The peak is indexed to the Ag-(111) plane and indicates that the film has a composite structure consisting of nanocrystalline face-centered cubic Ag phase embedded in an amorphous matrix. The SEM

Table 2
Sheet resistance, optical transmittance and figure of merit of furnace-annealed IAZ films with various AZ compositions.

		Rs (Ω/□)	T (%)	ϕ_{TC} (Ω^{-1})
100 °C	IA2Z	1170.0	49.5	7.5×10^{-7}
	IA3Z	998.0	46.9	5.2×10^{-7}
	IA5Z	486.0	40.2	2.3×10^{-7}
	IA6Z	37.8	60.0	1.6×10^{-4}
200 °C	IA2Z	985.5	51.4	1.3×10^{-6}
	IA3Z	879.7	47.2	6.2×10^{-7}
	IA5Z	379.1	48.2	1.8×10^{-6}
	IA6Z	33.3	62.7	2.8×10^{-4}
300 °C	IA2Z	1070.0	50.6	1.0×10^{-6}
	IA3Z	985.5	48.6	7.5×10^{-7}
	IA5Z	306.4	53.5	6.3×10^{-6}
	IA6Z	47.2	68.4	4.8×10^{-4}
400 °C	IA2Z	1440.0	65.6	1.0×10^{-5}
	IA3Z	1140.0	60.2	5.5×10^{-6}
	IA5Z	882.0	54.0	2.4×10^{-6}
	IA6Z	82.3	71.5	4.3×10^{-4}

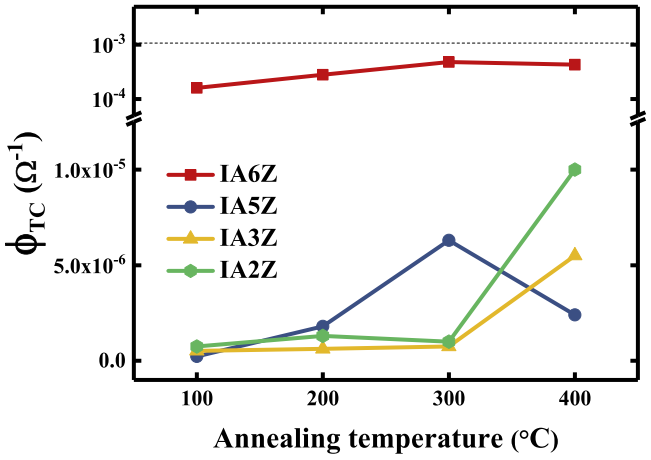

Fig. 6. Figure of merit values of furnace annealed FA IAZ films.

images presented in Fig. 2 show that the A5Z sample and A6Z sample both have a smooth surface without crystalline features. It is noted that this observation is consistent with the results presented previously for ITO/CuMg and ITO/ZrCu thin films in [18,19,40].

Fig. 3 presents the cross-sectional TEM images of the as-deposited A2Z and IA6Z samples. The images show that both films have a relatively smooth and continuous structure. Previous studies have shown that smooth and continuous structures are beneficial in enhancing the opto-electronic properties of similar monolithic and bi-layer structures [18]. Fig. 3(c) shows that the as-deposited ITO film has an amorphous structure. Overall, Figs. 2 and 3 show that the present AZ and IAZ films possess a relatively smooth and continuous structure even though they have a thickness of only ~10 nm. In other words, the present TFMG/TFMGC films are suitable candidates for minimizing the usage of ITO in multi-layer electrodes while maintaining good optoelectronic properties.

Fig. 4 shows the sheet resistance and optical transmittance properties of the as-deposited AZ samples as a function of the Ag content. As shown, the sheet resistance decreases with an increasing Ag content, i.e. from 1050 Ω/□ for the $Ag_{23}Zr_{77}$ sample to 195 Ω/□, for the $Ag_{66}Zr_{34}$ sample. By contrast, the transmittance of the AZ films increases slightly (from 44.5% to 47.5%) as the Ag content increases. In general, the results indicate that the electrical and optical properties of the as-deposited AZ films are both improved with a higher Ag addition. Table 1 shows the sheet resistance, transmittance and figure of merit values for all of the as-deposited AZ and IAZ films. It is seen that the sheet resistance of the IAZ films is lower than that of their AZ counterparts. For example, given an Ag content of 23 at%, the IA2Z film

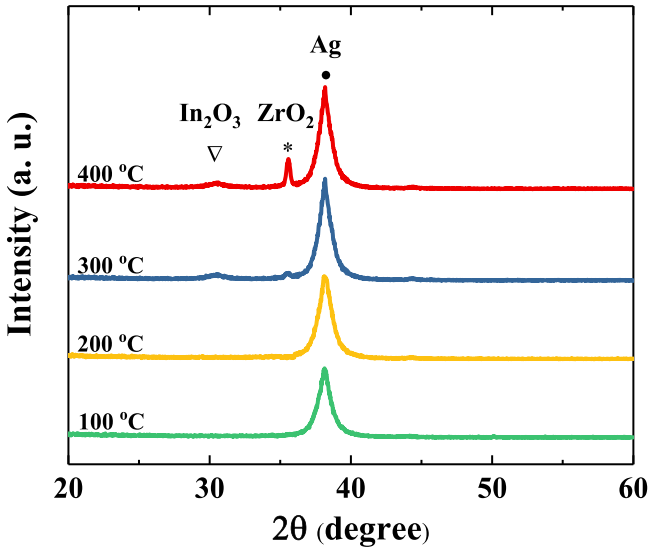

Fig. 7. XRD scans of IA6Z films processed by FA at different temperatures.

has a sheet resistance of 927 Ω/□, while the A2Z film has a resistance of 1050 Ω/□. For both types of film (i.e. monolithic and bi-layer), the sheet resistance decreases with an increasing Ag content. Comparing the two different types of film, it is seen that the bi-layer structures have a higher optical transmittance than the monolithic films. The present results are thus consistent with those reported in previous studies for ITO/CuMg systems [18,19]. Fig. 5 shows the figure of merit values for all the as-deposited AZ and IAZ films. The results confirm that, for a given Ag content, the bi-layer films provide a better optoelectronic performance than the monolithic films. Moreover, among all of the films, the IA6Z film achieves the best performance with a figure of merit equal to 2.0×10^{-5}.

3.2. Furnace annealing effects

Table 2 shows the sheet resistance, optical transmittance and figure of merit values of the IAZ bi-layer films furnace annealed at temperatures of 100–400 °C. The results show that a high annealing temperature (400 °C) leads to a significant increase in the sheet resistance; particularly in the samples with a higher Ag content. For the IA5Z and IA6Z samples, the figure of merit and transmittance are improved when using annealing temperatures of 300 and 400 °C, respectively. Fig. 6 presents the figure of merit values for all the furnace annealed IAZ films. Among all the films, the IA6Z film annealed at 300 °C has the highest figure of merit (i.e. 4.8×10^{-4} Ω^{-1}). In particular, the annealing process increases the optical transmittance by approximately 23% compared to the as-deposited sample (55.7% to 68.4%; see Tables 1 and 2) and reduces the sheet resistance by around 68% (145.8 Ω/□ to 47.2 Ω/□).

Fig. 7 shows the XRD patterns of the IA6Z films annealed at temperatures of 100~400 °C. For annealing temperatures of 300 °C or more, the XRD patterns contain both In_2O_3 and ZrO_2 crystalline peaks. Fig. 8 presents the TEM characterization results for the IA6Z film processed at the optimal annealing temperature of 300 °C. The selected area electron diffraction (SAED) pattern shown in Fig. 8(b) confirms that the annealed IA6Z film contains many crystalline phases, including In_2O_3, ZrO_2 and Ag. By contrast, the SAED pattern in Fig. 3(c) shows that the pure ITO film deposited on the AZ layer has a fully amorphous structure in the as-deposited condition. In other words, the ITO and AZ film change from an amorphous structure to a crystalline structure during the annealing process. Among the crystalline phases shown in Fig. 8(b), ZrO_2 possesses low electrical conductivity, and therefore accounts for the increased sheet resistivity of the samples annealed at temperatures of 300 or 400 °C. However, crystalline In_2O_3 is beneficial in improving the optical transmittance [29]. Consequently, the optical transmittance of the annealed film is improved due to presence of ZrO_2 and In_2O_3.

3.3. Laser annealing effects

Table 3 shows the sheet resistance, optical transmittance and figure of merit values for the IAZ films laser-annealed with a repetition rate of 150 kHz and pulse energies ranging from 1.0~2.5 μJ. For a given Ag content, the sheet resistance decreases and the transmittance increases with an increasing pulse energy. Similarly, for a given pulse energy, the sheet resistance reduces as the Ag content increases, while the transmittance increases. As for the LA samples, the IA6Z film achieves the highest figure of merit, irrespective of the pulse energy. Fig. 9 shows the figure of merit values for the IA6Z film given pulse energies of 2.0 μJ and 2.5 μJ and various values of the repetition rate in the range of 100~400 kHz. It is seen that the optimal annealing parameters are a pulse energy of 2.5 μJ and a repetition rate of 150 kHz. From Table 3, the corresponding values of the optical transmittance and sheet resistance are 64.0% and 17.8 Ω/□, respectively. Moreover, the figure of merit is equal to 6.5×10^{-4} Ω^{-1}. In other words, the optimal LA processing conditions result in a 32.5-fold improvement in the Haacke figure of merit compared to that of the IA6Z film in the as-deposited condition (2.0×10^{-5}, see Table 1). Fig. 10 shows the TEM characterization results for the optimal IA6Z sample laser annealed with a pulse energy of 2.5 μJ and a repetition rate of 150 kHz. The SAED pattern shows that the IA6Z sam-

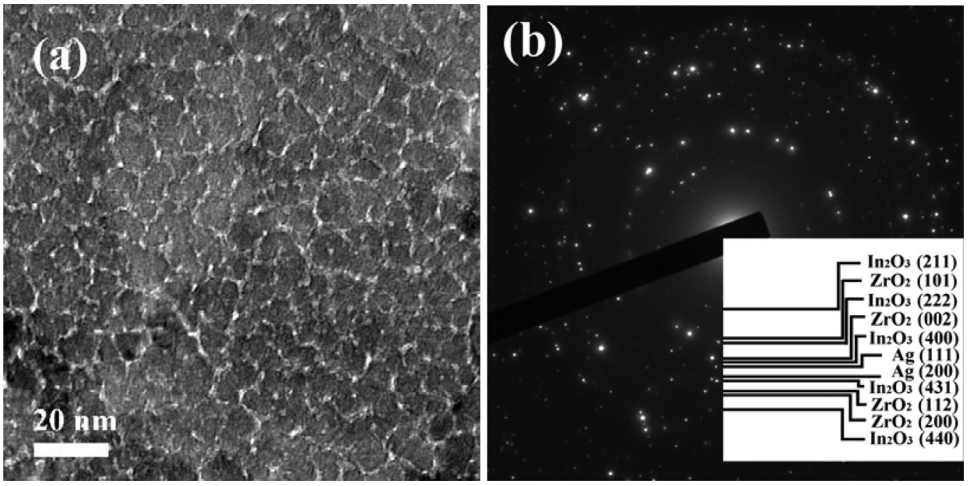

Fig. 8. TEM characterization results for IA6Z film processed by FA at 300 °C: (a) bright field image, and (b) corresponding SAED.

Table 3
Sheet resistance, optical transmittance and figure of merit of laser-annealed IAZ films with various AZ compositions at a repetition rate of 150 kHz. (Note that laser repetition rate is 150 kHz.).

		Rs (Ω/□)	T (%)	ϕ_{TC} (Ω^{-1})
1.0 μJ	IA2Z	1120.0	45.7	3.6×10^{-7}
	IA3Z	1222.0	46.1	3.6×10^{-7}
	IA5Z	135.0	48.5	4.7×10^{-6}
	IA6Z	22.9	60.5	2.9×10^{-4}
1.5 μJ	IA2Z	1060.0	46.4	4.4×10^{-7}
	IA3Z	990.0	45.8	4.1×10^{-7}
	IA5Z	122.4	51.0	9.7×10^{-6}
	IA6Z	22.7	61.2	3.2×10^{-4}
2.0 μJ	IA2Z	953.7	47.1	5.6×10^{-7}
	IA3Z	706.0	47.1	7.6×10^{-7}
	IA5Z	104.4	52.9	1.6×10^{-5}
	IA6Z	20.7	63.4	5.1×10^{-4}
2.5 μJ	IA2Z	803.7	48.1	8.3×10^{-7}
	IA3Z	481.0	47.7	9.8×10^{-7}
	IA5Z	93.6	51.2	1.3×10^{-5}
	IA6Z	17.8	64.0	6.5×10^{-4}

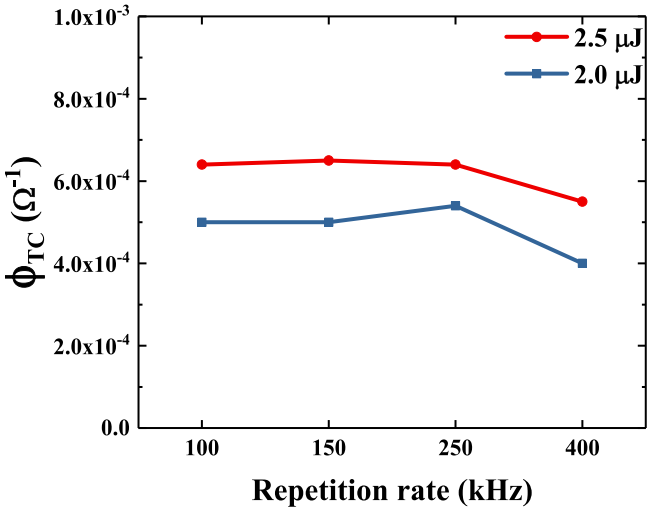

Fig. 9. Figure of merit results for I6AZ films processed by LA with different pulse energies and repetition rates.

ple contains many phases, including In_2O_3 (222), In_2O_3 (400), In_2O_3 (440), Ag (111), and Ag (200) (see Fig. 10(b)). Notably, compared to the FA sample, the laser-annealed IA6Z sample contains no ZrO_2 crystalline phase. This finding is reasonable since the LA process is characterized by an intense, but ultrafast, heating of the sample surface, which limits the time available for oxide generation.

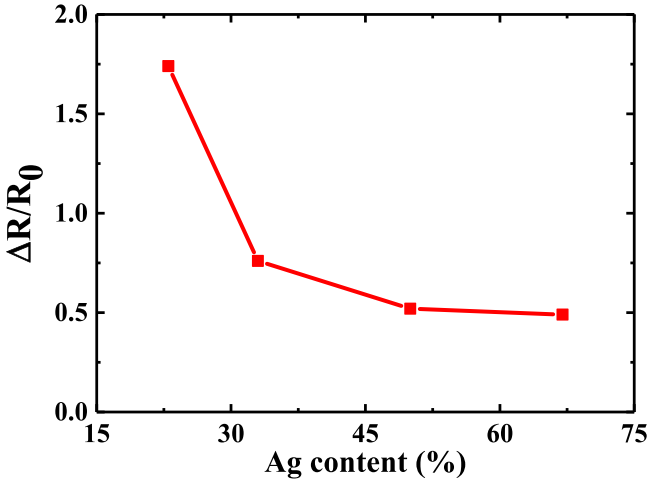

Fig. 11. Relative change in resistivity ($\Delta R/R_0$) of as-deposited IAZ films following fatigue tests (10,000 cycles) with bending radius of 7 mm.

Fig. 11 shows the change in resistivity ($\Delta R/R_0$, where R_0 is the initial resistivity, R_i is the measured resistivity after 10,000 cycles, and ΔR is R_i - R_0) of the as-deposited IAZ films following fatigue testing with a bending radius of 7 mm. It is seen that the change in resistivity increases with a decreasing Ag content. Previous studies have reported that the $\Delta R/R_0$ value for a pure ITO film with a thickness of 30 nm is around 0.93 [41]. Thus, the results presented in Fig. 11 show that the majority of the IAZ films have a more stable electrical resistivity than the pure ITO film under bending. For example, the $\Delta R/R_0$ value of the IA6Z film is just 0.49 following 10,000 bending cycles. The improvements of $\Delta R/R_0$ in the current films are quite pronounced.

4. Conclusions

This study has examined the optoelectronic properties of monolithic Ag-Zr (AZ) and bi-layer ITO/Ag-Zr (IAZ) thin films deposited on glass substrates and then processed by furnace annealing and laser annealing. Among all the as-deposited films, the $Ag_{66}Zr_{34}$ IAZ film achieves the best overall performance, i.e. an optical transmittance of 55.7% and an electrical resistivity of 145.8 Ω/□. The corresponding figure of merit is equal to 2.0×10^{-5} Ω^{-1}. Following furnace annealing at 300 °C,

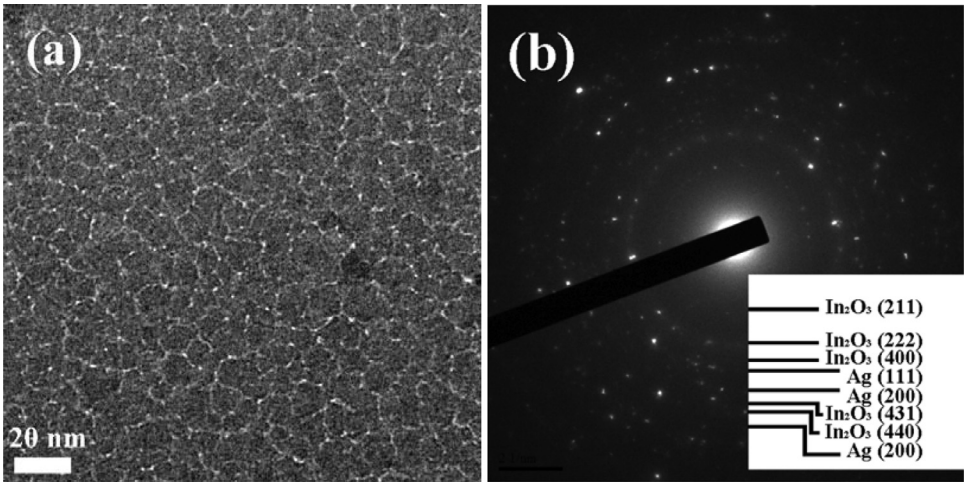

Fig. 10. TEM characterization results for IA6Z film processed by LA with pulse energy of 2.5 μJ: (a) bright field image, and (b) corresponding SAED.

the $Ag_{66}Zr_{34}$ IAZ film has an optical transmittance of 68.4% (i.e. 23% higher than the as-deposited film) and a sheet resistance of 47.2 Ω/□ (i.e. 68% lower than the as-deposited film). The corresponding figure of merit is equal to 4.8×10^{-4}. Given the optimal laser annealing parameters (i.e. a pulse energy of 2.5 μJ and a repetition rate of 150 kHz), the $Ag_{66}Zr_{34}$ IAZ film has a transmittance of 64.0% and a sheet resistance of 17.8 Ω/□. The corresponding figure of merit is equal to 6.5×10^{-4}. This value is higher than that for the optimal FA process (4.8×10^{-4}). Thus, it is inferred that the laser annealing process results in better optical and electrical properties than the furnace annealing process. Finally, the relative change in resistivity ($\Delta R/R_0 = 0.49$) of the as-deposited $Ag_{66}Zr_{34}$ IAZ sample following 10,000 bending cycles with a bend radius of 7 mm is significantly lower than that of a pure ITO film of roughly equivalent thickness ($\Delta R/R_0 = 0.93$). In other words, the bi-layer IAZ structure not only yields good optoelectronic properties, but also improves the bending fatigue resistance compared to a pure ITO film.

Acknowledgements

The authors gratefully acknowledge the financial support provided to this study by the Ministry of Science and Technology of Taiwan, ROC, under MOST 105-2221-E-110-019-MY3 and MOST 105-2221-E-020-007, and the City University of Hong Kong under Grant No. 9380088.

Supplementary materials

Supplementary material associated with this article can be found, in the online version, at doi:10.1016/j.optlaseng.2018.11.009.

References

[1] Lee BH, Iee Gon K, Sung Woo C, Lee SH. Effect of process parameters on the characteristics of indium tin oxide thin film for flat panel display application. Thin Solid Films 1997;302:25–30.
[2] Chang HW, Kim YH, Lee J, Hofmann S, Lüssem B, Müller-Meskamp L, Gather MC, Leo K, Wu CC. Color-stable, ITO-free white organic light-emitting diodes with enhanced efficiency using solution-processed transparent electrodes and optical outcoupling layers. Org Electron 2014;15:1028–34.
[3] Kim H, Gilmore CM, Piqué A, Horwitz JS, Mattoussi H, Murata H, Kafafi ZH, Chrisey DB. Electrical, optical, and structural properties of indium–tin–oxide thin films for organic light-emitting devices. J Appl Phys 1999;86:6451–61.
[4] Kloppel A, Meyer B, Trube J. Influence of substrate temperature and sputtering atmosphere on electrical and optical properties of double silver layer systems. Thin Solid Films 2001;392:311–14.
[5] Ahn MH, Cho ES, Kwon SJ. Effect of the duty ratio on the indium tin oxide (ITO) film deposited by in-line pulsed DC magnetron sputtering method for resistive touch panel. Appl Surf Sci 2011;258:1242–8.
[6] Kim HJ, Seo KW, Kim YH, Choi J, Kim HK. Direct laser patterning of transparent ITO–Ag–ITO multilayer anodes for organic solar cells. Appl Surf Sci 2015;328:215–21.
[7] Guillén C, Herrero J. ITO/metal/ITO multilayer structures based on Ag and Cu metal films for high-performance transparent electrodes. Sol Energy Mater Sol Cells 2008;92:938–41.
[8] egory OJG, Qing Luo EEC. High temperature stability of indium tin oxide thin films. Thin Solid Films 2002;406:286–93.
[9] Granqvist CG. A. Hulta˚ker, Transparent and conducting ITO films: new developments and applications. Thin Solid Films 2002;411:1–5.
[10] C. Guillén, J. Herrero, Comparison study of ITO thin films deposited by sputtering at room temperature onto polymer and glass substrates, Thin Solid Films, 480-481 (2005) 129–132.
[11] Lee J, Jung H, Lee J, Lim D, Yang K, Yi J, Song WC. Growth and characterization of indium tin oxide thin films deposited on PET substrates. Thin Solid Films 2008;516:1634–9.
[12] Ali AH, Shuhaimi A, Hassan Z. Structural, optical and electrical characterization of ITO, ITO/Ag and ITO/Ni transparent conductive electrodes. Appl Surf Sci 2014;288:599–603.
[13] Choi KH, Kim JY, Lee YS, Kim HJ. ITO/Ag/ITO multilayer films for the application of a very low resistance transparent electrode. Thin Solid Films 1999;341:152–5.
[14] Minami T. Present status of transparent conducting oxide thin-film development for Indium-Tin-Oxide (ITO) substitutes. Thin Solid Films 2008;516:5822–8.
[15] Guillén C, Herrero J. Transparent conductive ITO/Ag/ITO multilayer electrodes deposited by sputtering at room temperature. Opt Commun 2009;282:574–8.
[16] Kim JH, Kang TW, Kwon SN, Na SI, Yoo YZ, Im HS, Seong TY. Transparent conductive ITO/Ag/ITO electrode deposited at room temperature for organic solar cells. J Electron Mater 2016;46:306–11.
[17] Kim TH, Park SH, Kim DH, Nah YC, Kim HK. Roll-to-roll sputtered ITO/Ag/ITO multilayers for highly transparent and flexible electrochromic applications. Sol Energy Mater Sol Cells 2017;160:203–10.
[18] Lin HK, Cheng KC, Huang JC. Effects of laser annealing parameters on optical and electrical properties of ITO/Metallic glass alloy bi-layer films. Nanoscale Res Lett 2015;10:982.
[19] Lin HK, Hong SZ. Effects of Mg content and annealing treatment on optical and electrical properties of CuMg and ITO/CuMg metallic glass films. J Alloys Compd 2018;731:248–52.
[20] Diyatmika W, Chu JP, Kacha BT, Yu C-C, Lee C-M. Thin film metallic glasses in optoelectronic, magnetic, and electronic applications: a recent update. Curr Opin Solid State Mater Sci 2015;19:95–106.
[21] Pan CT, Chen YC, Lin PH, Hsieh CC, Hsu FT, Lin PH, Chang CM, Hsu JH, Huang JC. Lens of controllable optical field with thin film metallic glasses for UV-LEDs. Opt Express 2014;22:14411–24.
[22] Pan CT, Chen YC, Yang TL, Lin P-H, Lin P-H, Huang JC. Study of reflection–typed LED surgical shadowless lamp with thin film Ag-based metallic glass. Optik 2016;127:2193–6.
[23] Danışman M. The corrosion behavior of nanocrystalline nickel based thin films. Mater Chem Phys 2016;171:276–80.
[24] Chang CM, Yang CJ, Wang KK, Liu JK, Hsu JH, Huang JC. On the reflectivity and antibacterial/antifungal responses of Al-Ni-Y optical thin film metallic glass composites. Surf Coat Technol 2017;327:75–82.
[25] Lin YT, Chung YL, Wang ZK, Huang JC. AgMgAl metallic glassy and intermetallic thin films for electric contact applications. Intermetallics 2015;57:133–8.
[26] Sahu DR, Chen CY, Lin SY, Huang J-L. Effect of substrate temperature and annealing treatment on the electrical and optical properties of silver-based multilayer coating electrodes. Thin Solid Films 2006;515:932–5.
[27] Bu IYY. A simple annealing process to obtain highly transparent and conductive indium doped tin oxide for dye-sensitized solar cells. Ceram Int 2014;40:3445–51.
[28] Lin HK, Hsu WC. Electrode patterning of ITO thin films by high repetition rate fiber laser. Appl Surf Sci 2014;308:58–62.
[29] Lee CJ, Lin HK, Li CH, Chen LX, Lee CC, Wu CW, Huang JC. A study on electric properties for pulse laser annealing of ITO film after wet etching. Thin Solid Films 2012;522:330–5.
[30] Wang S, Ouyang X, Feng Z, Cao Y, Gu M, Li X. Diffractive photonic applications mediated by laser reduced graphene oxides. Opto-Electron Adv 2018;1:17000201–8.
[31] El hamali SO, Cranton WM, Kalfagiannis N, Hou X, Ranson R, Koutsogeorgis DC. Enhanced electrical and optical properties of room temperature deposited Aluminium doped Zinc Oxide (AZO) thin films by excimer laser annealing. Opt Lasers Eng 2016;80:45–51.
[32] Tao XY, Fsaifes I, Koncar V, Dufour C, Lepers C, Hay L, Capoen B, Bouazaoui M. CO2 laser-induced crystallization of sol–gel-derived indium tin oxide films. Appl Phys A 2009;96:741–9.
[33] Shin H, Sim B, Lee M. Laser-driven high-resolution patterning of indium tin oxide thin film for electronic device. Opt Lasers Eng 2010;48:816–20.
[34] Tseng SF, Hsiao WT, Chiang D, Huang KC, Chou CP. Mechanical and optoelectric properties of post-annealed fluorine-doped tin oxide films by ultraviolet laser irradiation. Appl Surf Sci 2011;257:7204–9.
[35] Chen MF, Lin KM, Ho YS. Laser annealing process of ITO thin films using beam shaping technology. Opt Lasers Eng 2012;50:491–5.
[36] Wang CM, Huang CC, Kuo JC, Huang JL. Investigation of pulsed ultraviolet laser annealing of Sb/SnO2 thin films on the structural, optical and electrical properties. Surf Coat Technol 2013;231:374–9.
[37] Huang LJ, Ren NF, Li BJ, Zhou M. Improvement in overall photoelectric properties of Ag/FTO bilayer thin films using furnace/laser dual annealing. Mater Lett 2014;116:405–7.
[38] Benware BR, Macchietto CD, Moreno CH, Rocca JJ. Demonstration of a high average power tabletop soft X-Ray laser. Phys Rev Lett 1998;81:5804–7.
[39] Haacke G. New figure of merit for transparent conductors. J Appl Phys 1976;47:4086.
[40] Lee CJ, Lin HK, Sun SY, Huang JC. Characteristic difference between ITO/ZrCu and ITO/Ag bi-layer films as transparent electrodes deposited on PET substrate. Appl Surf Sci 2010;257:239–43.
[41] Lin HK, Chiu SM, Cho TP, Huang JC. Improved bending fatigue behavior of flexible PET/ITO film with thin metallic glass interlayer. Mater Lett 2013;113:182–5.